Supplemental material for *Invariant forms of dissolution fingers*

Stanisław Żukowski,[1,2] Silvana Magni,[1] Florian Osselin,[3] Filip Dutka,[1] Max Cooper,[1] Anthony J. C. Ladd,[4] and Piotr Szymczak[1]

[1] *Institute of Theoretical Physics, Faculty of Physics, University of Warsaw, Pasteura 5, 02-093 Warsaw, Poland*
[2] *Laboratoire Matière et Systèmes Complexes (MSC), UMR 7057, CNRS & Université Paris Cité, 10 rue Alice Domon et Léonie Duquet, 75013 Paris, France*
[3] *Institut des Sciences de la Terre, Orleans, France*
[4] *Chemical Engineering Department, University of Florida, Gainesville FL 32611, USA*

Here we derive equations describing the invariant propagation of a dissolution finger in a Hele-Shaw cell with a soluble base. A sketch of the experimental cell [1] is shown in the paper (Fig. 2). Fluid is injected in the narrow gap between the inert (polycarbonate) top layer and the soluble (gypsum) bottom layer (Figs. 2 b-c). The gypsum layer near the inlet dissolved rapidly (Fig. 2b), on a timescale of about 10 hours, to create a step profile extending over a distance of the order of 1 mm (Fig. 2c). The profile is uniform in the transverse (y) direction and at first propagates slowly downstream, on timescales up to a few days [1]. However, over longer times perturbations appear in the front (Fig. S1a), which eventually develop into well formed fingers (Fig. S1 b-c) that slowly coarsen over time. Results from those experiments are shown in Figs. 1b, 3, and 5. This document is largely a compendium of published results, which we have assembled for the convenience of readers desiring a more in depth description of the physics outlined in the main paper.

I. GOVERNING EQUATIONS

Gypsum dissolution,

$$\mathrm{CaSO_4(s)} \rightarrow \mathrm{Ca^{2+}} + \mathrm{{SO_4}^{2-}}, \tag{1}$$

has a particularly simple kinetics [2], which to a good approximation is linear in the undersaturation of calcium ions, $c = c_{\mathrm{sat}} - [\mathrm{Ca^{2+}}]$. The dissolution rate (the number of dissolved molecules per unit area and unit time) is then

$$R(c) = kc, \tag{2}$$

where k is the reaction rate constant, which can include corrections for the diffusional hindrance across the concentration boundary layer. A similar, product-controlled reaction kinetics is also appropriate for other minerals, such as halite (dissolved by water) or limestone dissolved by groundwater [3]. The rate constant for gypsum dissolution by distilled water is $k = 4.5 \times 10^{-4}$ cm/s [2, 4].

The dissolution reaction on the gypsum surface gives rise to an increase in aperture,

$$\partial_t h = \alpha k c \theta(h_{\max} - h), \tag{3}$$

where $\alpha = \nu_{\mathrm{m}}/(1-\varphi)$ is the volume (per mole) occupied by the solid phase; it is determined by the molar volume (ν_{m}) and the porosity (φ) of the soluble material [1]. The function θ is a step function; $\theta(x) = 1$ if $x > 0$ and zero otherwise. The large volume of solution needed to dissolve a given volume of mineral establishes a time scale separation between changes in aperture and the evolution of the flow and concentration fields, which can therefore be treated as stationary [5].

The thin film (or lubrication) approximation is used to describe flow and reactant transport in the Hele-Shaw cell. The average velocity $\boldsymbol{v}$ and concentration c are related to integrals over the aperture:

$$\boldsymbol{v}h = \int_0^h \boldsymbol{u}\mathrm{d}z, \qquad \boldsymbol{v}hc = \int_0^h \boldsymbol{u}c\mathrm{d}z, \tag{4}$$

where $\boldsymbol{u}(x,y,z)$ is the three-dimensional flow field. After integrating over the fracture aperture (z-direction):

$$\boldsymbol{v} = -\frac{h^2}{12\eta}\boldsymbol{\nabla} p, \tag{5}$$

$$\boldsymbol{\nabla}\cdot(\boldsymbol{v}hc) = \boldsymbol{\nabla}\cdot(Dh\boldsymbol{\nabla}c) - kc\,\theta(h_{\max} - h), \tag{6}$$

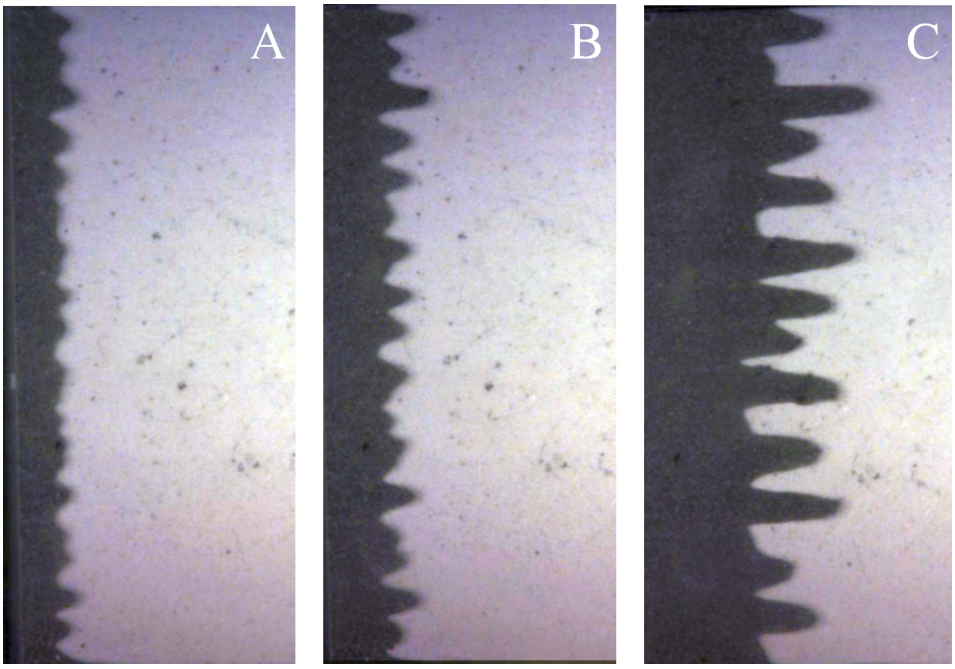

Figure S1. Evolution of the dissolution patterns in the microfluidic experiments. The flow enters from the left and progressively dissolves the gypsum block. The front between the dissolved area (black) and the undissolved area (white) becomes unstable, causing the dissolution to focus into fingers.

where $\boldsymbol{\nabla}$ is the two-dimensional (xy) gradient operator. We ignore the numerically small distinction between the velocity averaged concentration, which appears in the convective flux, and the average concentration in the diffusive flux [6].

Although equations (3)–(6) have a simple solution, with a uniform reactive front $h(x,t)$ propagating from inlet to outlet, they are linearly unstable to transverse perturbations in the aperture field [7]. Over time the front breaks down into interacting fingers (Fig. S1) with a wavelength controlled by the flow and reaction rate. The wavelength calculated from linear stability analysis [8] is in good agreement with the initial dissolution patterns observed experimentally [1]. In the later stages of evolution, the fingers begin to interact with each other. Two processes take place: one is the competition of the fingers for the flow, causing the longer ones to advance ahead of the shorter ones. The other is the merging of the fingers, reducing their total number. As a result, as shown in Fig. S1, the pattern coarsens. In the long-time limit, a single finger would emerge. However, observing the entire dynamics – from the formation of the initial instabilities to the emergence of one or two fingers – would require experiments in a very long system, which is technically unfeasible. Therefore, to analyze the interaction between two fingers or the growth of a single finger, we initialize growth in specific (y) locations by making small cuts in the gypsum at the inlet. The cuts are placed symmetrically, either a single one at the centerline of the system (for one-finger systems) or two at equal distances from the centerline (for two-finger systems).

Equation (6) can be written in dimensionless form by scaling coordinates with the width of the channel W, velocity by its average value $v_0 = Q_{\rm tot}/(W h_{\rm max})$, aperture by $h_{\rm max}$, and concentration by $c_{\rm sat}$. Denoting the scaled variables with a hat, the dimensionless Eq. (6) is:

$$\mathrm{Pe}\,\hat{\boldsymbol{\nabla}}\cdot(\hat{\boldsymbol{v}}\hat{h}\hat{\boldsymbol{\nabla}}\hat{c}) = \hat{\boldsymbol{\nabla}}\cdot\hat{h}\hat{\boldsymbol{\nabla}}\hat{c} - \mathrm{Da}\,\hat{c}, \tag{7}$$

where

$$\mathrm{Da} = \frac{kW^2}{Dh_{\rm max}}, \tag{8}$$

and

$$\mathrm{Pe} = \frac{v_0 W}{D} = \frac{Q_{\rm tot}}{Dh_{\rm max}}. \tag{9}$$

II. INVARIANT FINGERS

Equations (3)-(6) allow for invariant solutions for the aperture field in the coordinate system comoving with the finger tip:

$$\tilde{x} = x - x_{\rm tip}(t). \tag{10}$$

The aperture evolution, Eq. (3), in this coordinate system is

$$-U(t)\partial_{\tilde{x}} h = \alpha k c \theta (h_{\rm max} - h), \tag{11}$$

where $U(t) = {\rm d}x_{\rm tip}/{\rm d}t$. If h is to be invariant in the comoving frame, then $\partial_{\tilde{x}} h$ is time independent, which implies that the concentration field depends on time only through $U(t)$. Since in the comoving frame c can be written as a product of time and space dependent functions, and h is time independent, it follows from Eq. (6) that the flow field $\boldsymbol{v}$ must also be time-independent in the comoving frame. Thus the shape of the finger can remain invariant, even when the propagation velocity $U(t)$ is changing in time.

III. THIN-FRONT LIMIT

Away from the tip, the thickness of the interface between dissolved and undissolved material is controlled by the balance between diffusion of reactant from the fully dissolved finger body, which is of the order of $Dh_{\rm max}\partial_y^2 c$, and the rate of consumption as the reactant encounters the undissolved solid, kc. The reactant is consumed over a length scale $\sqrt{Dh_{\rm max}/k} \approx 0.05$ cm, which is much smaller than the width of the finger body (≈ 1 cm). Hence, we can replace the aperture field by a boundary separating fully dissolved ($h = h_{\rm max}$) and entirely undissolved ($h = h_0$) material. Within the finger there is no reaction, and Eq. (6) from the SM reduces to Eq. (3) in the paper. Outside the boundary, the water is fully saturated ($c = 0$). The state of the system is then specified by the position of the boundary, $x_{\rm f}(y,t)$, and the invariance condition reduces to Eq. (1) in the paper.

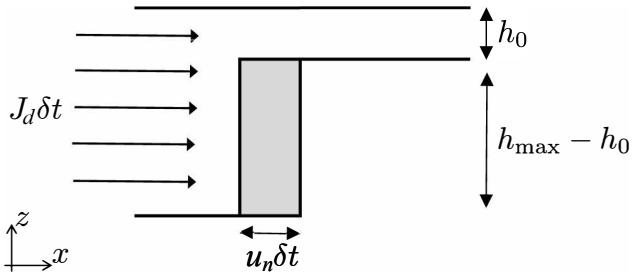

Figure S2. Cross section of the system in xz plane in the thin-front limit. Over the time interval δt, $J_d\delta t$ molecules of the reactant (per unit length in the y direction) dissolve the volume of $\nu_{\rm m} J_d \delta t$ of the mineral (marked in gray), which can also be expressed as $(1-\varphi)(h_{\rm max} - h_0)u_n \delta t$. The comparison of both expression for the dissolved volume leads to Eq. (12).

In the thin-front limit, the advancement of the boundary between the phases is linked to the flux of reactant at a given point $\boldsymbol{r}_{\rm f} = (x_{\rm f}(y), y)$

$$u_n = \boldsymbol{n} \cdot \frac{{\rm d}\boldsymbol{r}_{\rm f}}{{\rm d}t} = -\frac{\alpha}{(h_{\rm max} - h_0)} D h_{\rm max} \left(\nabla c\right)_n , \tag{12}$$

where the subscript n indicates the component normal to the interface. Only the (depth-integrated) diffusive flux $J_{\rm d} = -Dh_{\rm max}\nabla c$ is present in Eq. (12). Since the concentration at the front vanishes, so does the convective contribution to the flux. The front velocity (12) is then obtained from the flux by observing that the total volume dissolved by the reactant crossing the reaction front over a time δt, can be expressed, on one hand, as $\nu_{\rm m} J_{\rm d} \delta t$, and, on the other, as $(1-\varphi)(h_{\rm max} - h_0)u_n \delta t$ (see Fig. S2).

IV. INVARIANT FINGERS IN THREE DIMENSIONS

For the interpretation of natural forms, such as the solution pipes shown in Fig. 1 or Fig. S3, we must consider three spatial dimensions. Here, the invariance condition becomes

$$U\pi a^2 = \alpha Q \bar{c}, \tag{13}$$

while the transport equation is now

$$\frac{\partial(v_x c)}{\partial x} = D\frac{1}{r}\frac{\partial}{\partial r}r\left(\frac{\partial c}{\partial r}\right), \tag{14}$$

where x is the axial direction of the pipe, r is the radial coordinate and $a(x)$ is the radius of the pipe. If the pipe is treated as locally uniform, Eq. (14) can again be solved by separation of variables. For the slowest decaying mode

$$c(r,x) = \frac{\bar{c}(x) j_{0,1}}{2J_1(j_{0,1})} J_0\left(j_{0,1}\frac{r}{a}\right), \tag{15}$$

where J_n denotes a Bessel function of the first kind, and $j_{0,1}$ is the first zero of J_0. Similarly to the two-dimensional case, we will use this solution also for a nonuniform radius, $a(x)$, assuming that $\mathrm{d}a/\mathrm{d}x \ll 1$.

Combining an integration over r of Eq. (14),

$$(Q\bar{c})' = -D\pi\bar{c}(j_{0,1})^2, \tag{16}$$

with the invariance condition (13) gives the shape equation:

$$\frac{\mathrm{d}a}{\mathrm{d}x} = -\frac{\pi a D}{2Q}(j_{0,1})^2. \tag{17}$$

Figure S3. Group of soil-filled solution pipes in Canunda National Park, Australia. The photo is courtesy of Ken Grimes.

[1] F. Osselin, A. Budek, O. Cybulski, P. Kondratiuk, G. P., and P. Szymczak, Microfluidic observation of the onset of reactive in infiltration instability in an analog fracture, Geophys. Res. Lett. **43**, 6907 (2016).

[2] J. Colombani, Measurement of the pure dissolution rate constant of a mineral in water, Geochim. Cosmochim. Acta **72**, 5634 (2008).

[3] L. N. Plummer, T. L. M. Wigley, and D. L. Parkhurst, The kinetics of calcite dissolution in CO2-water systems at 5 °C to 60 °C and 0.0 to 1.0 atm of CO2, Am. J. Sci. **278**, 537 (1978).

[4] F. Dutka, V. Starchenko, F. Osselin, S. Magni, P. Szymczak, and A. J. C. Ladd, Time-dependent shapes of a dissolving mineral grain: comparisons of simulations with microfluidic experiments, Chem. Geol. **540**, 119459 (2020).

[5] A. J. C. Ladd and P. Szymczak, Use and misuse of large-density asymptotics in the reaction-infiltration instability, Water Resour. Res. **53**, 2419 (2017).

[6] V. Balakotaiah, Hyperbolic averaged models for describing dispersion effects in chromatographs and reactors, Korean J. Chem. Eng. **21**, 318 (2004).
[7] P. Szymczak and A. J. C. Ladd, The initial stages of cave formation: Beyond the one-dimensional paradigm, Earth Planet. Sci. Lett. **301**, 424 (2011).
[8] P. Szymczak and A. J. C. Ladd, Reactive-infiltration instabilities in rocks. Fracture dissolution, J. Fluid Mech. **702**, 239 (2012).